

A Comparison of Finite-Time and Finite-Size Lyapunov Exponents

Ronald Peikert, Armin Pobitzer, Filip Sadlo, and Benjamin Schindler

Abstract Finite-time and finite-size Lyapunov exponents are related concepts that have been used for the purpose of identifying transport structures in time-dependent flow. The preference for one or the other concept seems to be based more on a tradition within a scientific community than on proven advantages. In this study, we demonstrate that with the two concepts highly similar visualizations can be produced, by maximizing a simple similarity measure. Furthermore, we show that results depend crucially on the numerical implementation of the two concepts.

1 Introduction

The finite-time Lyapunov exponent (FTLE) has been proposed by Haller [13] as an indicator of Lagrangian coherent structures (LCSs). The finite-size Lyapunov exponent (FSLE) is an alternative and especially popular in oceanography [9, 19]. It seems that the preference for FTLE or FSLE is based more on the tradition within a particular scientific community than on an evaluation of the two approaches. Direct comparisons between FTLE and FSLE have been made by Boffetta et al. [5] and by Sadlo and Peikert [21]. Boffetta argued that the FTLE is not capable of recognizing the relevant structures, namely the boundaries between chaos and large-scale mixing

R. Peikert (✉) • B. Schindler
Department of Computer Science, ETH Zurich, Zurich, Switzerland
e-mail: peikert@inf.ethz.ch; bschindler@inf.ethz.ch

A. Pobitzer
University of Bergen, Bergen, Norway
e-mail: armin.pobitzer@uib.no

F. Sadlo
University of Stuttgart, Stuttgart, Germany
e-mail: Filip.Sadlo@visus.uni-stuttgart.de

regime. A recent paper by Karrasch and Haller [16] lists a number of theoretical limitations of FSLE and proposes the use of infinitesimal-time Lyapunov exponents.

We show, based on two examples, that FTLE and FSLE, if appropriately calibrated, produce comparable results which can be interchangeably used for most purposes in numerical flow visualization. However, in terms of computational effort FTLE is slightly more efficient, because computation can be based on a single precomputed flow map. In oceanographic research, FSLE and FTLE are typically computed from particle pairs consisting of horizontal or vertical pairs of grid points. This means a quantization of the range of directions into a set of only four directions. As we show, the effect of this quantization is that FTLE and FSLE values are underestimated by a factor which can be large, especially for short integration times. We give an example where this factor is unbounded.

Another important algorithmic aspect is the correct choice of a scale, given a grid resolution. There are two approaches to FSLE and FTLE computation, both of which require a scale parameter. In methods based on particle pairs, this is the initial separation of the particles. In methods based on the Cauchy-Green tensor, a scale is needed in gradient estimation. We demonstrate the effect of the scale parameter.

We define a similarity measure for pairs of FTLE and FSLE images, based on which image pairs can be computed using an optimization process. For a given FTLE or FSLE image, a corresponding image of the other field can be produced. We discuss results of this process in Sects. 5 and 6.

2 Related Work

Particle transport is a central feature of fluid flows. In this context, the investigation of mixing properties and the existence of transport barriers is of great interest, e.g., for the distribution of chemicals in the atmosphere [18] or in a bay area [8].

Transport barriers and mixing can be studied by means of the local attracting or repelling properties of trajectories. These properties are connected to the concept of *stable* and *unstable manifolds* in dynamical systems [12, 26]. Along these lines, Haller proposed FTLE as a quantification method of these properties [12, 13]. FTLE is a finite-time version of the well-known *Lyapunov exponent* [11]. An alternative is the *finite-size Lyapunov exponent*, as described by Boffetta et al. [5].

In the same paper, Boffetta et al. [5] compare FSLE to FTLE and two Eulerian-based techniques for the identification of transport barriers in two-dimensional incompressible fluids. The comparison is angled towards geophysical flows, like ocean currents and atmospheric flows. The authors conclude that both FSLE and FTLE are superior to the Eulerian-based methods in uncovering the transport barriers. Furthermore, they find FSLE to be more expressive for large-scale transport, while FTLE captures mainly small-scale properties of the particle dispersion. It is worthwhile noticing that the comparison conducted by Boffetta et al. is based on particle pairs, and may hence be affected by sampling issues. We comment on this issue in Sect. 3.3.1. Joseph and Legras [15] cite Haller [12] stating that

the distribution of pair separation is typically a “fuzzy” view of the hyperbolic manifolds. They claim that FSLE results in a less fuzzy distribution and allows the manifold structures to emerge more naturally.

While FSLE is usually preferred in the analysis of mixing and transport in oceans [9, 15] and atmosphere [18], FTLE has been applied to these domains as well. Coulliette et al. [8] make use of FTLE to investigate the existing transport barriers in a bay area in order to achieve optimal timing for the relief of contaminants into the bay. Beron-Vera et al. [4] identify so-called *invariant tori*, which act as transport barriers, in geophysical flows by means of FTLE. Üffinger et al. [25] compare the FTLE computation based on linearization and dense direction sampling. They conclude that a dense sampling of directions produces more accurate results than the classical approach based on linearization, while preserving its advantages in the detection of topological features.

3 Finite-Time and Finite-Size Lyapunov Exponents

Given a velocity field $\mathbf{u}(\mathbf{x}, t)$, the *flow map* $\Phi_t^{t+\tau}(\mathbf{x})$ describes the advection of a “particle” released at time t and location \mathbf{x} over a time span τ . Both t and the integration time τ are considered to be parameters, hence the flow map is mapping from the spatial domain to itself, mapping initial locations to final locations.

3.1 Intuitive Definitions

Given a particle seeded at location \mathbf{x} and time t , and advected over time τ , the *dispersion* of a neighbor particle seeded at \mathbf{y} is observed. The location \mathbf{y} is chosen on a sphere of radius d around \mathbf{x} , such that the dispersion is maximized. This leads to the definition of the *finite-time Lyapunov exponent* at location \mathbf{x} and time t , for a given integration time τ , which is

$$FTLE_\tau(\mathbf{x}, t) = \lim_{d \rightarrow 0} \max_{\|\mathbf{y}-\mathbf{x}\|=d} \frac{1}{|\tau|} \ln \frac{\|\Phi_t^{t+\tau}(\mathbf{y}) - \Phi_t^{t+\tau}(\mathbf{x})\|}{d}. \quad (1)$$

For a given *dispersion factor* r , the *finite-size Lyapunov exponent* [1] at location \mathbf{x} and time t is:

$$FSLE_r(\mathbf{x}, t) = \lim_{d \rightarrow 0} \max_{\|\mathbf{y}-\mathbf{x}\|=d} \frac{1}{|\tau_r|} \ln r \quad (2)$$

where τ_r is the minimum time for which

$$\left\| \Phi_t^{t+\tau_r}(\mathbf{y}) - \Phi_t^{t+\tau_r}(\mathbf{x}) \right\| / d = r. \quad (3)$$

3.2 Equivalent Definitions

The above equations contain a maximization over directions and a limit, which both have to be approximated in computation. This can be avoided by using the equivalent definitions [7]

$$FTLE_\tau(\mathbf{x}, t) = \frac{1}{|\tau|} \ln \sqrt{\lambda_{\max}(\mathbf{C}_t^{t+\tau}(\mathbf{x}))} \quad (4)$$

where $\mathbf{C}_t^{t+\tau}(\mathbf{x}) = \nabla \Phi_t^{t+\tau}(\mathbf{x})^* \nabla \Phi_t^{t+\tau}(\mathbf{x})$ is the (right) Cauchy-Green tensor, and

$$FSLE_r(\mathbf{x}, t) = \frac{1}{|\tau_r|} \ln r \quad (5)$$

where $|\tau_r|$ is the minimum time for which

$$\sqrt{\lambda_{\max}(\mathbf{C}_t^{t+\tau_r}(\mathbf{x}))} = r. \quad (6)$$

3.3 Computation Based on Particle Pairs

One approach to FTLE and FSLE computation is the explicit use of particle pairs, according to the definitions from Sect. 3.1. The limits occurring in Eqs. (1) and (2) are approximated in practice by choosing a small d , while maximization is approximated by testing a finite set of directions. While for a good approximation quality sufficiently many directions are needed, it is established practice to use only the four grid neighbors [14].

The approach based on Eqs. (1) and (2) is popular especially in the oceanography community for FSLE computation. D’Ovidio et al. [9] describe the investigation of mixing structures in the Mediterranean sea by FSLE, using a four neighbor-based approximation of the maximal growth rate of particle separation. FSLE is used to identify hyperbolic points, which indicate areas of strong mixing. The authors point out the natural compatibility of FSLE with data collected by *Lagrangian drifters*, and the possibility to suppress small-scale mixing by the dispersion factor r .

Hernández-Carrasco et al. [14] discuss the reliability of FSLE with respect to sampling density for particles seeding and the grid resolution of the underlying velocity field. While noting the theoretical need to investigate “all” possible separation directions, also their computations consider two directions only. They find that FSLE are consistent under grid refinement for both seed point and velocity field, while the amount of details captured increases with finer resolution.

Fig. 1 FTLE of the velocity field $u = y, v = x$, computed with particle pairs on uniform grid. For larger τ they converge to the correct value of 1.0

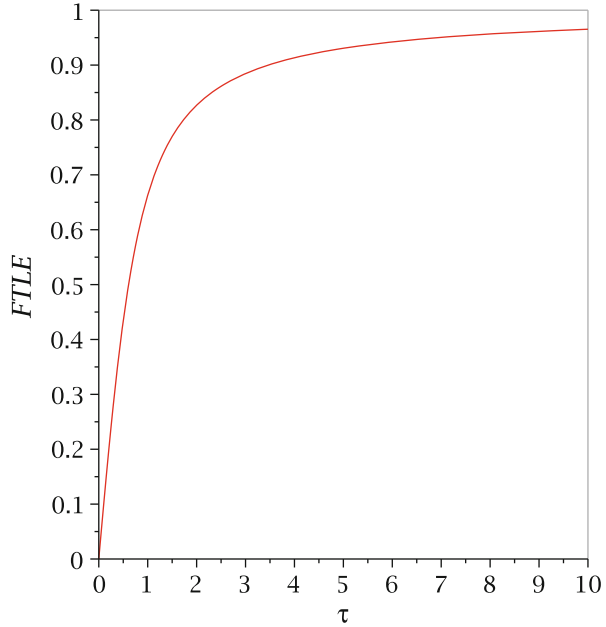
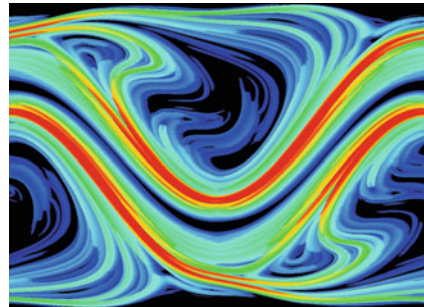


Fig. 2 Effects of quantization of directions: Same as Fig. 6a, but with computation based on particle pairs (four neighbors only)



3.3.1 Shortcoming of the Computation Based on Four Neighbors

Using the simple linear velocity field $u = x, v = -y$, we demonstrate that computation using only four neighbors can lead to large errors in FTLE (and FSLE) values. The flow map of the field after integration time τ is $\Phi_0^\tau(x, y) = (xe^\tau, ye^{-\tau})$, its right Cauchy-Green tensor is $diag(e^{2\tau}, e^{-2\tau})$, and finally, the FTLE is the constant 1. Two particles seeded at $(0, 0)$ and $(h, 0)$ are mapped to $(0, 0)$ and $(he^\tau, 0)$, therefore $r = e^\tau$, and the particle-based method gives the correct result. A wrong result is obtained, however, if a 45° rotation is applied to the velocity field. Then, the seed points $(\pm h, 0)$ and $(0, \pm h)$ are mapped to $(\pm h \cosh \tau, \pm h \sinh \tau)$ and $(\pm h \sinh \tau, \pm h \cosh \tau)$, respectively, therefore $r = \sqrt{\cosh(2\tau)}$, and the FTLE value is $\ln \cosh(2\tau)/2\tau$, which deviates from 1 especially for small τ , as is shown in Fig. 1. Such quantization artifacts in an FSLE computation are shown in Fig. 2.

In order to reduce this error, one would have to use a finer quantization of directions. This could be done by using auxiliary particles on a circle around the reference particle as in [25].

3.4 Computation Based on the Cauchy-Green Tensor

Errors due to quantization of directions are eliminated if the definitions from Sect. 3.2 are used. This is at the cost of errors introduced by gradient estimation, which are typically much smaller. Therefore, computation based on the Cauchy-Green tensor is the preferred method both in the fluid dynamics and the scientific visualization community [7, 20, 24]. The first stage of the method is to sample the flow map, which requires a high-quality numeric integrator. The sampling grid can be chosen independent of the discretization of the velocity data, therefore, a uniform regular grid is typically used. In the second stage, the flow map gradient is estimated at each sample position, and Eqs. (4) or (5) is used to generate the final values.

3.5 Scale Considerations

Both of the above approaches contain a “scale” parameter which affects the computed scalar field. In Sect. 3.3 this is the distance d between particle pairs, while in Sect. 3.4 a distance d is needed for gradient estimation using, e.g., finite differences. For setting the parameter d , in either one of its meanings, there are two opposite approaches:

1. By choosing d very small, a good approximation of the FTLE or FSLE at the point \mathbf{x} is obtained. Accuracy can be further improved with Benettin’s *renormalization* algorithm [2], where during integration particles are reset to a fixed distance from the reference particle. Renormalization was originally used for computing (non-finite) Lyapunov exponents. A variant of renormalization is the L-FTLE proposed by Kasten et al. [17], where numerical integration and differentiation are swapped. While pointwise exact, these methods may miss thin ridges of high values passing between samples. Even without renormalization, using a d smaller than the sampling distance creates artifacts, since it is equivalent to first computing the FTLE or FSLE field at sampling distance d and then doing a subsampling, which obviously causes aliasing in the presence of high frequencies. This type of artifacts can be noticed in Fig. 5 of [5].
2. By choosing d in the order of the sampling distance, the obtained FTLE or FSLE values are less accurate, but they are representative for the space between samples. This results in unbroken ridges, which is a requirement for subsequent ridge extraction. Figure 6b has been produced using gradient estimation from a 5-point finite-difference stencil. For the fine structures, resulting from the

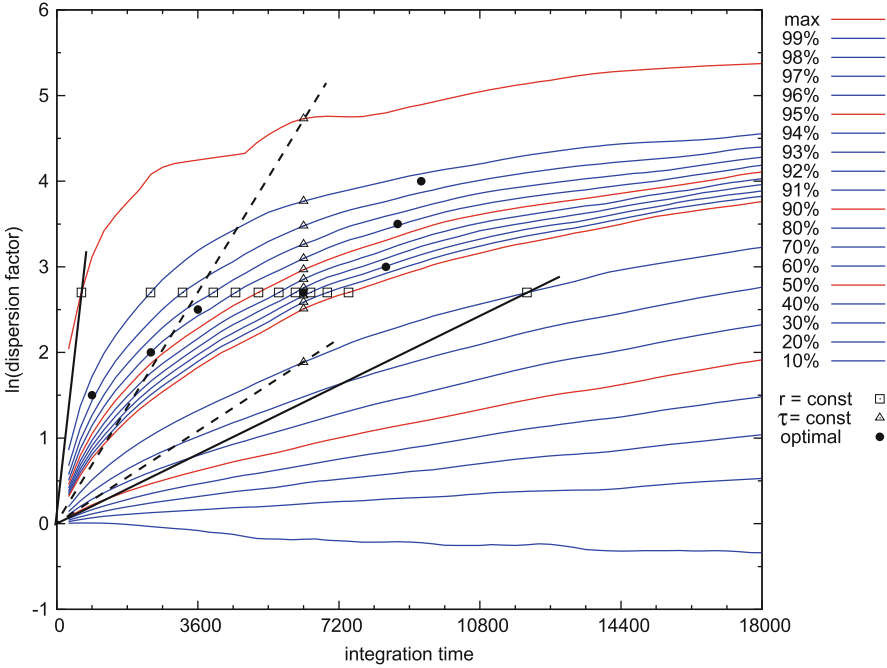


Fig. 3 Percentiles of $\ln(r)$ as functions of integration time of the Vattestraumen data (with forward integration). FTLE (FSLE) values are obtained by taking a vertical (horizontal) section. The actual values are the slopes of the *dashed (solid) lines* passing through the origin and the respective point. The *filled circles* mark a few pairs (τ, r) , where for a given integration time τ the dispersion factor r has been computed which maximizes the similarity measure

long integration time, the chosen d is barely sufficient to avoid aliasing. For even longer integration a smaller d would be needed [10]. The same holds if subsequent ridge extraction is needed, where it is advantageous to compute gradients by convolution with derivatives of a Gaussian [23].

4 Comparing FTLE and FSLE Images

Computation of FSLE samples on a given grid can be done by simultaneous integration of trajectories and computing the dispersion factors r after each integration step. This way, a function $r(\tau)$ is obtained, from which both FTLE and FLSE can be derived, by computing $\ln(r(\tau))/|\tau|$ for some fixed τ or fixed r , respectively. Figure 3 shows percentiles of $\ln(r)$, computed for the data set of Sect. 6 on a 868 by 868 grid. At each point (x, y) in this plot, the actual FTLE or FSLE value is given by the slope y/x . Taking a vertical section (marked with triangles) yields percentiles of FTLE values for this integration time, while a horizontal section (marked with boxes) yields FLSE values for the corresponding r . In the example FTLE at $\tau = 6,300$ s and FSLE at $\ln(r) = 2.7$ are shown.

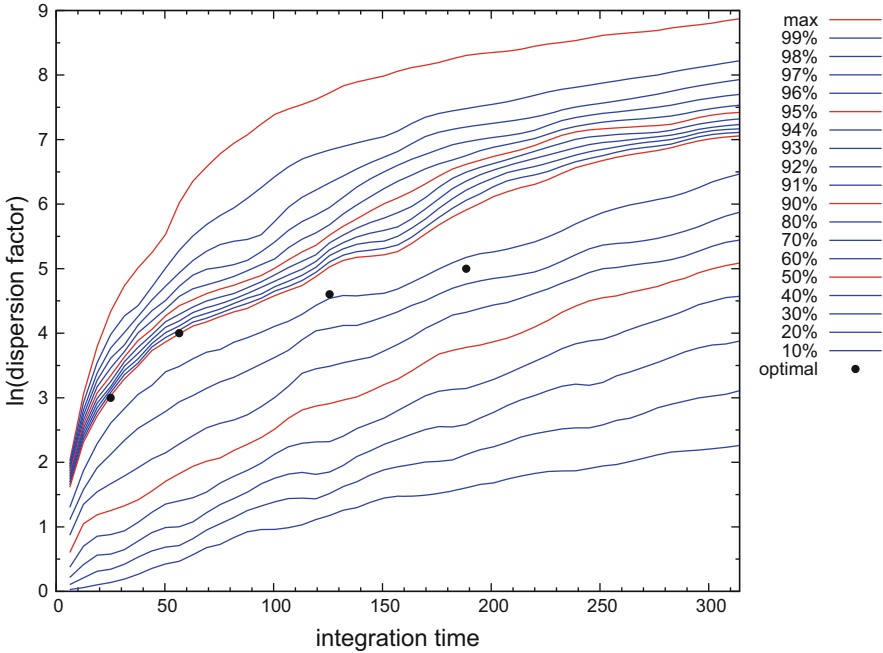


Fig. 4 Percentiles and optimal parameter pairs for meandering jet model. $(\omega, \epsilon) = (0.1, 0.3)$

The fact that the horizontal line does not intersect some of the curves indicates that for some of the trajectories the dispersion factor r has not been reached. At these points, an FSLE sample cannot be computed within the given maximum integration time (here $\tau_{max} = 18,000$), but it is known to be less than $\ln r / \tau_{max}$. For visualization purposes, a value of either 0 or $\ln r / \tau_{max}$ can be assigned to such points.

While FSLE and FTLE values are the same at the point where the vertical and horizontal lines intersect, their range is in general different. In our example in Fig. 3 the range between the 80- and 100-percentiles is wider for FSLE (marked with solid lines) than for FTLE values (marked with dashed lines).

We observed this difference in all velocity fields that we tested. A similarity measure for comparing FTLE and FSLE fields has to account for this difference. Therefore, the straightforward choice is to define the *similarity* of a pair of fields $f(\mathbf{x}) = FTLE_r(\mathbf{x})$ and $g(\mathbf{x}) = FSLE_r(\mathbf{x})$ as their correlation

$$\text{corr}(f, g) = \text{cov}(f, g) / \sqrt{\text{var}(f) \text{var}(g)}. \quad (7)$$

Given one FTLE or FLSE field, a matching field of the other type can now be found by maximizing the similarity. A few such pairs are represented in Figs. 3 and 4 by filled circles. Such optimal pairs, resulting from maximization of similarity, are shown in Figs. 6 and 7.

In principle, it is possible to maximize similarity over both parameters simultaneously. However, this tends to result in extreme parameter values, which are not

practically usable. By manually choosing one of the two parameters, the user can balance the visualization with respect to the length and “sharpness” of structures and the amount of folding.

Typically, only the higher FTLE or FSLE values are of interest, therefore the transfer function should clamp data at a lower threshold. Furthermore, to account for the different ranges of FTLE and FSLE data, the transfer function should either be based on normalized data or on percentiles. We chose the second approach, and we clamped the analytic data in Sect. 5 at the 50-percentile and the numerical data in Sect. 6 at the 90-percentile, meaning that we focused on the highest 10 % of FTLE and FSLE values. Which percentile range is of interest depends on the data, or more precisely, on the size and frequency of transport barriers. The percentile plots (Figs. 3 and 4) can then be used to map the chosen percentile range to a range in the parameters τ or r . Finally, a fast heuristic way to avoid the brute-force optimization would be to define the midpoints of these two ranges as a matching parameter pair (τ, r) . However we experienced that the similarity values obtained this way were in some cases not near the optimum.

5 Analytic Test Case: The Meandering Jet Model

Bower [6] introduced an analytic flow field for studying the mixing behavior of oceanic jets. Its stream function is defined as

$$\psi = -\tanh\left(\frac{y - B \cos kx}{\sqrt{1 + (kB \sin kx)^2}}\right) + cy. \quad (8)$$

The velocity components are then $u = -\frac{\partial\psi}{\partial y}$, $v = \frac{\partial\psi}{\partial x}$. This flow is steady in the moving frame where it is formulated. Samelson [22] derived an unsteady version of it by making the meander amplitude B depend on time:

$$B = B_0 + \epsilon \cos(\omega t). \quad (9)$$

The stream function of the flow, at times $t = 0$ and $t = 10\pi$ (where the amplitude takes its maximum and minimum) is shown in Fig. 5. Parameter values have been chosen as $B_0 = 1.2$, $L = 10.0$, $k = 2\pi/L$, $c = 0.1$, $\omega = 0.1$ and $\epsilon = 0.3$. In these images, contour lines are the streamlines of the velocity field.

5.1 Comparison of FTLE and FSLE

The meandering jet flow has been used by Boffetta et al. [5] in their comparison of FTLE and FSLE. They used Samelson’s model with parameters $B_0 = 1.2$, $L = 10.0$, $k = 2\pi/L$ and $c = 0.1$. For the parameter pair (ω, ϵ) the two settings

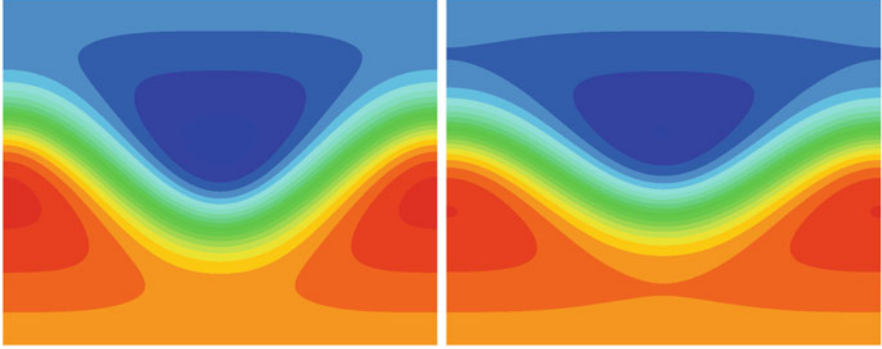


Fig. 5 Stream function of the meandering jet ($0 \leq x \leq 10, -4 \leq y \leq 4$) at $t = 0$ (left) and $t = 10\pi$ (right)

(0.1, 0.3) and (0.4, 0.3) were investigated. The resulting images have led the authors to the conclusion that FSLE is preferable over FTLE, because the FTLE image (Fig. 4 in [5]) fails to discern the structures seen in the FSLE image (Fig. 5 in [5]).

We reproduced FTLE and FSLE images for the same parameter settings, but using computation based on the Cauchy-Green tensor. In order to obtain comparable structures, it is necessary to adjust the parameters of each technique, i.e., the integration time τ for FTLE and the dispersion factor r for FSLE. For this purpose we used the similarity measure from Sect. 4. Starting from the FSLE parameter $r = 100$, used in [5] (see their Fig. 2a), we obtained first the FSLE image Fig. 6a. Then, a maximally similar FTLE image 6b was obtained for the parameter value $\tau = 40\pi$ (having tested only multiples of 2π). Boffetta et al. were using an integration time of only $\tau = 4\pi$ for their FTLE image (see their Fig. 4a in [5]). The reason for the unsharp FTLE structures is clearly the short integration time, which does not match well the parameter chosen for the FSLE image. Our FTLE result for a short integration time ($\tau = 8\pi$) is shown in Fig. 6d, and we obtained a similar FSLE image for $\ln(r) = 3$ in Fig. 6c.

Aliasing artifacts, which are present in Boffetta's FSLE images, can be avoided by using a sufficient mesh resolution. We used 1,000 by 800, as compared to the 10,000 points mentioned in [5]. Another difference to be noted is that Fig. 4a in [5] is missing the glide reflection symmetry, which is present in the underlying velocity field. The explanation given for this is the dependency on the phase of the flow. However, we obtained an FTLE field having the correct symmetry for all tested phase shifts.

Finally, FSLE computation requires as a secondary parameter a maximum integration time $|\tau_{max}|$. If this is exceeded, this means that the FSLE value can be at most $\ln(r)/|\tau_{max}|$, and it is set to zero (black color in Fig. 6a, c). Choosing $|\tau_{max}|$ too small results in missing structures at lower FSLE values.

By computing FTLE and FSLE from the Cauchy-Green tensor and choosing pairs of parameters based on our proposed similarity measure, comparable structures can be found in this test data. This holds for long (Fig. 6a, b) and short (Fig. 6c, d) integration times.

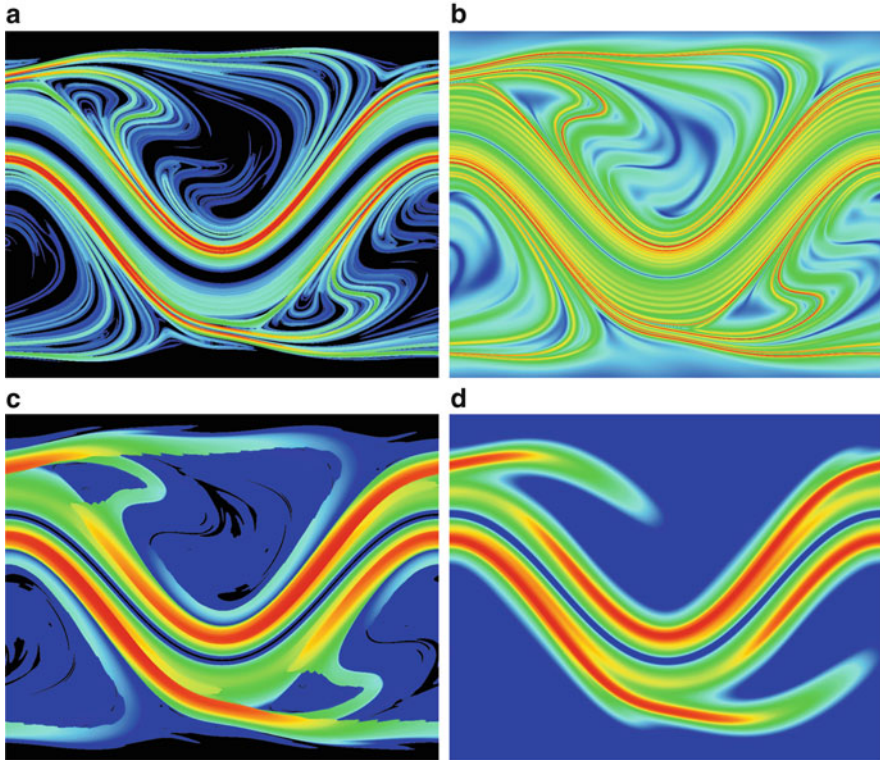


Fig. 6 Meandering jet with $(\omega, \epsilon) = (0.1, 0.3)$, FSLE and FTLE computed with two methods. (a) FSLE computed with Cauchy-Green tensor. Time $t = 0$, dispersion factor $r = 100$, maximum time 100π (five flow periods). Color map: 0.01 (blue) to 0.1 (red). (b) FTLE computed with Cauchy-Green tensor. Time $t = 0$, integration time $\tau = 40\pi$ (two flow periods). Color map: 0.01 (blue) to 0.055 (red). (c) Same as Fig. 6a, but with $r = e^3 \approx 20.1$. (d) Same as Fig. 6b, but with shorter integration time $\tau = 8\pi$

6 Numerical Test Case: Tidal Flow in a Narrow Passage

Our second test case is a CFD simulation of the tidal flow in the *Vatlestraumen* passage, which is a part of the main shipping lane to the harbor of Bergen, Norway. After a tragic naval accident in 2004, the tidal flow in the passage has been modeled with the *Bergen Ocean Model* (BOM) [3]. The data set used in this comparison study is a simulation of approximately one full tidal cycle (12 h). The simulation itself is 3D, but only the surface layer was used for the study. The surface layer flow is the essential one for, e.g., pollution by fuel leaking from the vessel. The time resolution of the data set is 30 s, internally the simulation uses a time step of 1.5 s.

While in this kind of application FSLE is typically used, highly similar structures are obtained with FTLE, as Fig. 7 proves. At least the strong ridges (colored red) can be recognized in the corresponding image, even though colors can differ.

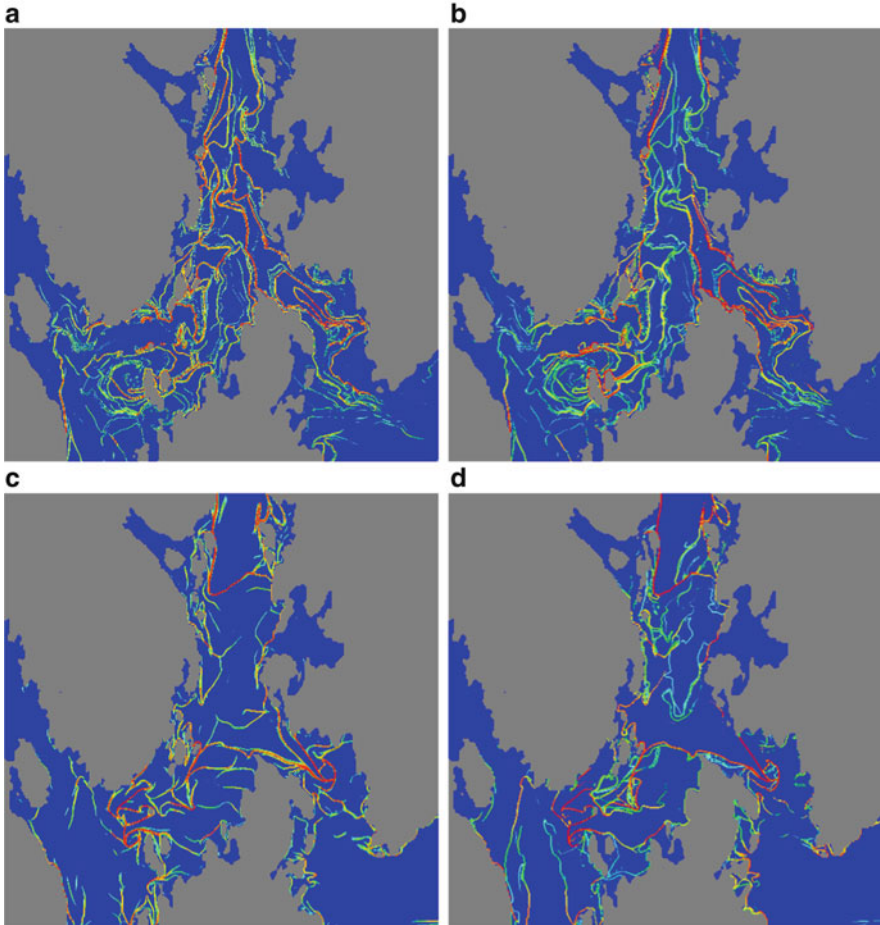


Fig. 7 Comparison of FTLE and FSLE in tidal flow. **(a)** Forward (repelling) FTLE, integration time $\tau = 2\text{h}20'$. **(b)** Forward (repelling) FSLE, dispersion factor $r = \exp(3.00)$. **(c)** Backward (attracting) FTLE, integration time $\tau = -30'$. **(d)** Backward (attracting) FSLE, dispersion factor $r = \exp(3.00)$

7 Conclusion

Calibration of parameters can produce similar FTLE and FSLE fields and thus similar visualizations of the LCSs in a flow dataset. Differences still exist, and it would be a worthwhile goal to further analyze them. However, we showed that differences are less fundamental than was suggested in literature. Observed differences can be due to poor choice of parameters as well as sampling artifacts. Using our proposed calibration method, it is now possible to compare adequate pairs of fields and focus on the inherent differences of FTLE and FSLE. For this, pairs

of parameters τ and r have to be found such that the corresponding FTLE and FSLE fields are similar, i.e., highly correlated. An obvious, brute-force approach is to use an optimization strategy in order to maximize correlation. However, this requires repeated computation of such fields. For practical purposes, a faster method is needed. An interesting problem for future work would be to find a heuristic that is able to find near-optimal pairs of parameters.

While the actual results that can be achieved by FTLE and FSLE are rather similar, it is worthwhile noting the subtle conceptual difference between the two methods: The FSLE allows us, by the choice of the parameter r , to focus on local separation above a certain threshold. Additional information about the typical time-scale of the observed mixing/transport is also provided, which can be a valuable additional information [9, 14]. The FTLE, on the other hand, operate with a fixed time-scale and detect separation at all spatial scales. This allows us also to assess the interplay of the detected structures [26]. Depending on prior knowledge about the time- and spatial scales of interest for a specific application, as well as whether or not the interplay of structures is of interest, FTLE may be a more appropriate choice than FSLE, and vice versa.

Acknowledgements We wish to thank Tomas Torsvik, Uni Research, Uni Computing (Bergen, Norway), for the tidal flow data. This work was funded in part by the Seventh Framework Programme for Research of the European Commission, under FET-Open grant number 226042 (project SemSeg) and the Swiss National Science Foundation, under grant number 200020_140556.

References

1. E. Aurell, G. Boffetta, A. Crisanti, G. Paladin, A. Vulpiani, Growth of noninfinitesimal perturbations in turbulence. *Phys. Rev. Lett.* **77**, 1262–1265 (1996)
2. G. Benettin, L. Galgani, A. Giorgilli, J.M. Strelcyn, Lyapunov characteristic exponent for smooth dynamical systems and hamiltonian systems: a method for computing all of them. *Mechanica* **15**, 9–20 (1980)
3. J. Berntsen, User guide for a modesplit σ -coordinate ocean model. Version 4.1. Technical report, Department of Mathematics, University of Bergen, Norway, 2004
4. F.J. Beron-Vera, M.J. Olascoaga, M.G. Brown, H. Kocak, I.I. Rypina, Invariant-tori-like lagrangian coherent structures in geophysical flows. *Chaos* **20**(1), 1–13 (2010)
5. G. Boffetta, G. Lacorata, G. Redaelli, A. Vulpiani, Detecting barriers to transport: a review of different techniques. *Physica D* **159**, 58–70 (2001)
6. A. Bower, A simple kinematic mechanism for mixing fluid parcels across a meandering jet. *J. Phys. Oceanogr.* **21**, 173–171 (1991)
7. S. Brunton, C. Rowley, Fast computation of finite-time Lyapunov exponent fields for unsteady flows. *Chaos* **20**(017503), 017503-1–017503-12 (2010)
8. C. Coulliette, F. Lekien, J.D. Paduan, G. Haller, J.E. Marsden, Optimal pollution mitigation in monterey bay based on coastal radar data and nonlinear dynamics. *Environ. Sci. Technol.* **41**(18), 6562–6572 (2007)
9. F. d’Ovidio, V. Fernández, E. Hernández-García, C. López, Mixing structures in the Mediterranean Sea from finite-size Lyapunov exponents. *Geophys. Res. Lett.* **31**(17), L17203-1–L17203-4 (2004). doi:10.1029/2004GL020328

10. R. Fuchs, B. Schindler, R. Peikert, Scale-space approaches to FTLE ridges, in *Topological Methods in Data Analysis and Visualization II*, ed. by R. Peikert, H. Hauser, H. Carr, R. Fuchs (Springer, New York, 2012), pp. 283–296
11. I. Goldhirsch, P.L. Sulem, S.A. Orszag, Stability and Lyapunov stability of dynamical systems: a differential approach and a numerical method. *Physica D* **27**(3), 311–337 (1987)
12. G. Haller, Finding finite-time invariant manifolds in two-dimensional velocity fields. *Chaos* **10**(1), 99–108 (2000)
13. G. Haller, Distinguished material surfaces and coherent structures in three-dimensional fluid flows. *Physica D* **149**, 248–277 (2001)
14. I. Hernández-Carracos, C. López, E. Hernández-García, A. Turiel, How reliable are finite-size Lyapunov exponents for the assessment of ocean dynamics? *Ocean Model.* **36**(3–4), 208–218 (2011)
15. B. Joseph, B. Legras, Relation between kinematic boundaries, stirring, and barriers for the antarctic polar vortex. *J. Atmos. Sci.* **59**, 1198–1212 (2002)
16. D. Karrasch, G. Haller, *Do Finite-Size Lyapunov Exponents Detect Coherent Structures?* (2013). <http://arxiv.org/abs/1307.7888>
17. J. Kasten, C. Petz, I. Hotz, B. Noack, H.C. Hege, Localized finite-time lyapunov exponent for unsteady flow analysis, in *Vision Modeling and Visualization*, vol. 1, ed. by M. Magnor, B. Rosenhahn, H. Theisel (Universität Magdeburg, Inst. f. Simulation u. Graph., 2009), pp. 265–274
18. T.Y. Koh, B. Legras, Hyperbolic lines and the stratospheric polar vortex. *Chaos* **12**(2), 382–394 (2002)
19. A.J. Mariano, A. Griffa, T.M. Özgökmen, E. Zambianchi, Lagrangian analysis and predictability of coastal and ocean dynamics 2000. *J. Atmos. Ocean. Technol.* **19**(7), 1114–1126 (2002)
20. A. Pobitzer, R. Peikert, R. Fuchs, B. Schindler, A. Kuhn, H. Theisel, K. Matković, H. Hauser, The state of the art in topology-based visualization of unsteady flow. *Comput. Graph. Forum* **30**(6), 1789–1811 (2011)
21. F. Sadlo, R. Peikert, Efficient visualization of lagrangian coherent structures by filtered AMR ridge extraction. *IEEE Trans. Vis. Comput. Graph.* **13**(5), 1456–1463 (2007)
22. R. Samelson, Fluid exchange across a meandering jet. *J. Phys. Oceanogr.* **22**, 431–440 (1992)
23. B. Schindler, R. Peikert, R. Fuchs, H. Theisel, Ridge concepts for the visualization of lagrangian coherent structures, in *Topological Methods in Data Analysis and Visualization II*, ed. by R. Peikert, H. Hauser, H. Carr, R. Fuchs (Springer, New York, 2012), pp. 221–236
24. S.C. Shadden, F. Lekien, J.E. Marsden, Definition and properties of Lagrangian coherent structures from finite-time Lyapunov exponents in two-dimensional aperiodic flows. *Physica D: Nonlinear Phenom.* **212**(3–4), 271–304 (2005)
25. M. Üffinger, F. Sadlo, M. Kirby, C.D. Hansen, T. Ertl, FTLE computation beyond first order approximation, in *Eurographics Short Papers*, ed. by C. Andujar, E. Puppo, Eurographics Association, Cagliari, pp. 61–64, 2012
26. S. Wiggins, The dynamical systems approach to lagrangian transport in oceanic flows. *Annu. Rev. Fluid Mech.* **37**, 295–328 (2005)